bjh research paper

Myeloma impairs mature osteoblast function but causes early expansion of osteo-progenitors: temporal changes in bone physiology and gene expression in the KMS12BM model

Deepika Kassen,[1] Darren Lath,[2] Anna Lach,[1] Holly Evans,[2] Andy Chantry,[2] Neil Rabin,[1] Peter Croucher[3] and Kwee L. Yong[1]

[1]Department of Haematology, Cancer Institute, University College London, London, [2]Academic Unit of Bone Biology, University of Sheffield, Sheffield, UK and [3]Bone Biology Division, Garvan Institute of Medical Research, Sydney, NSW, Australia

Received 21 April 2015; accepted for publication 22 July 2015

Correspondence: Kwee L. Yong, Department of Haematology, UCL Cancer Institute, 72 Huntley Street, London WC1E 6BT, UK.
E-mail: kwee.yong@ucl.ac.uk

Summary

Myeloma bone disease results from an uncoupling of osteoclastic resorption and osteoblastic bone formation, but early changes in osteogenic function remain poorly defined. We used the KMS12BM xenograft model to investigate cellular and molecular events at early and late stages of disease. Lytic lesions and changes in osteoblast and osteoclast numbers occur late (8 weeks), however, micro-computed tomography of femora revealed significant reduction in bone volume at earlier disease stages (3 weeks) when tumour burden is low. Calcein labelling demonstrated reduced mineralization and bone formation at 3 weeks, suggesting functional impairment despite preserved osteoblast numbers. Osteo-progenitors from compact bone increased early (1 week), but fell at 3 weeks and were profoundly suppressed by 8 weeks. Exposure of osteoblast progenitors to multiple myeloma (MM) cells *in vitro* induced cell cycling, suggesting a mechanistic basis for early expansion of osteo-progenitors. We observed temporal changes in chemokine, osteogenic and osteoclastogenic genes in the stromal compartment. Notably, an early rise in CCL3 may underlie functional changes in mature osteoblasts at 3 weeks. Our data indicate that MM has distinct effects on mature osteoblasts and immature osteo-progenitors. Our findings argue for early clinical intervention to prevent bone changes that ultimately lead to the development of osteolytic disease.

Keywords: myeloma, osteoblast, stroma, osteo-progenitors.

A major clinical feature of multiple myeloma (MM) is osteolytic bone disease, which is present in up to 70% of patients, resulting in bone pain, fractures and vertebral collapse with or without cord compression, hypercalcaemia and osteoporosis. Central to disease pathogenesis is the ability of tumour cells to disrupt normal bone homeostasis. Coupled bone turnover is a process that is active throughout adult life, and is maintained by the opposing actions of osteoclasts and osteoblasts. The 'uncoupling' that occurs in MM results from increased osteoclast activity as well as suppressed osteoblast function, and the mechanisms underlying these phenomena have been the subject of intense study over many years (Roodman, 2009). Several osteoclastogenic cytokines have been identified, including interleukin (IL)-3, IL6 and chemokine (C-C motif) ligand 3 [CCL3, also termed macrophage inflammatory protein (MIP)-1α], many of which converge on the RANK/RANKL pathway, that is of central importance in osteoclast differentiation and activation (Giuliani *et al*, 2004). Osteoblast suppressive mechanisms, however, remain incompletely understood. Evidence indicates a role for soluble WNT antagonists (DKK1, sFRP), although not all studies support this, and other cytokines, such as hepatocyte growth factor, IL7, sclerostin and activin, have been implicated (Roodman, 2011; Bolzoni *et al*, 2013). The temporal changes at a cellular level, however, remain poorly defined. Osteoblasts differentiate from multipotent mesenchymal (stem) progenitor cells (MSC), going through the different stages of pre-osteoblast to become mature functional osteoblasts before becoming either embedded in bone as osteocytes or terminally

First published online 2 November 2015
doi: 10.1111/bjh.13790

© 2015 John Wiley & Sons Ltd

differentiated on the bone surface as bone lining cells (Heino & Hentunen, 2008). It remains unclear if impaired bone formation in MM is related to dysfunctional MSCs, a defect in early commitment to the osteoblast lineage, repression of the differentiation programme or the malfunction of mature osteoblasts.

Studies in MM patients with bone disease confirm increased osteoclast numbers and activity, reduced osteoblast numbers and bone formation rate, reduced markers of bone formation and increased markers of bone resorption (Valentin-Opran *et al*, 1982; Jakob *et al*, 2002; Terpos *et al*, 2010). These observations are often made at a late stage of disease, when bone loss has already occurred and lytic disease is widespread. Some insights into the early pathogenic processes in the development of myeloma bone disease come from histological studies in patients with early MM, where increased bone resorption was accompanied by an increase in bone formation rates, whereas in patients with more advanced disease, osteoblast activity was depressed, whilst osteoclast activity remained high (Bataille *et al*, 1991). These observations suggest that, initially, increased osteoblast recruitment maintains the coupling between bone resorption and formation but that this is lost in the later stages of disease, resulting in increased osteolysis (Taube *et al*, 1992; Bataille *et al*, 1995). Indeed, abnormalities of bone remodelling in patients with monoclonal gammopathy of undetermined significance (MGUS) are characterized by increased bone formation, as well as increased resorption (Bataille *et al*, 1996; Vejlgaard *et al*, 1997; Politou *et al*, 2004). However, these studies are based upon static histological assessments or serum markers of bone formation and dynamic cellular changes have not been determined. Failure of bone formation and repair is a feature of advanced disease, occurring as the culmination of a series of changes in the MM environment. The precise nature of these changes, and the actual cell types involved at different stages, is unclear.

In this study, we aimed to map the early cellular changes in osteoblast function that occur prior to the development of overt bone loss in MM. We studied temporal changes in mature osteoblast function by measuring dynamic bone formation, and we also studied changes in the progenitor [MSC/pre-osteoblast (pre-OB)] compartment *in vivo* prior to the development of osteolytic bone lesions. We employed the KMS12BM xenogeneic model, which we previously characterized (Rabin *et al*, 2007), because it resembles the human disease: predominant medullary pattern of disease, and recapitulation of key features of MM associated bone disease. Using luciferase-modified tumour cells to track the spatial and temporal progression of disease, we assessed time-dependent changes in bone morphology and metabolism, and functional changes in both the mature osteoblast and the immature progenitor (stromal/pre-OB) compartments so as to gain a fuller understanding of the early events in MM bone disease. Finally we examined the stromal compartment for temporal changes in expression of selected genes considered to play a role in tumour growth and bone disease.

Materials and methods

Animals

All procedures involving the use and care of animals were performed in accordance with the Animals Scientific Procedures Act (1986) and approved by the UCL/UCLH Joint Ethics Committee and licensed by the Home Office. Beta-2-microglobulin non-obese diabetic/severe combined immunodeficient (β_2m NOD/SCID) animals were housed under positive pressure in individually ventilated cages (Tecniplast, Northamptonshire, UK).

KMS12BM bioluminescence model

The KMS12BM cell line was kindly provided by Dr T Otsuki (Kawasaki Medical School, Okoyama, Japan). Cells were transduced using a bicistronic retrovirus containing the eBFP gene and sorted to obtain >99% transgene expressing cells (Fig S1). 10^7 Luciferase-transduced KMS12BM cells (10^7) in exponential growth were injected by tail vein into 8-week-old un-conditioned female β2M NOD/SCID mice. Animals were monitored weekly for disease progression using luciferase imaging. Based on initial experiments, cohorts of injected animals were sacrificed at 1, 3 and 8 weeks post-injection. Mice were injected i.p. with 30 mg/kg luciferin and imaged at 10 min post-injection using a Xenogen live animal imager with an exposure time of 1 s.

Immunohistochemistry

Paraffin-embedded femoral sections were stained with mouse anti-human plasma cell antibody (Clone VS38C, Dako, Ely, UK) using standard techniques (Rabin *et al*, 2007) to detect engrafted MM cells.

Micro-computed tomography analysis

The femora of mice injected with phosphate-buffered saline (PBS, control) or human myeloma cell lines KMS12BM and MM1s were scanned on a Skyscan microCT scanner (model 1172a, Skyscan, Antwerp, Belgium) at 50 kV and 200 μA using a 0·5 aluminium filter and a detection pixel size of 4·4 μm^2. Images were captured every 0·7° through 180° rotation of each bone. Scanned images were reconstructed using Skyscan NRecon software and analysed using the Skyscan computerized tomography (CT) analysis software. Trabecular bone was measured over a 1 mm^3 volume, 0·2 mm from the growth plate. Trabecular bone volume (BV) as proportion of tissue volume (BV/TV, %), trabecular thickness (Tb.Th, /mm^2), trabecular number (Tb.N, /mm), and structure model index (SMI) were assessed in this region using the CT analy-

© 2015 John Wiley & Sons Ltd

sis software. Lesions in cortical bone of femora were quantified and analysed using ImageJ (ImageJ.net) (Supporting Information).

Osteoblast and osteoclast analysis using static histomorphometry

Femora of mice injected with PBS (control) or the human myeloma cell line KMS12BM were fixed in 10% buffered formalin, processed through alcohols and embedded in paraffin wax. Two levels (50 μm apart) of 3-μm sections were cut onto Superfrost Plus slides (Fisher Scientific UK, Loughborough, UK) using a Leica RM2265 microtome with a stainless steel feather blade. Sections were stained for tartrate resistant acid phosphatase activity (TRAP) and examined using a DMRB light microscope (Leica, Milton Keynes, UK). Osteoblast and osteoclast number and perimeter were quantified on the cortico-endosteal and trabecular bone surfaces. For cortico-endosteal bone analysis, six 250 μm × 250 μm fields down each side of the bone were analysed with a total of 3 mm length, and with a starting point 250 μm from the growth plate. For trabecular bone analysis, an area measuring 0·75 mm^2, 250 μm from the growth plate was used. For osteoblasts, the percentage of bone covered by osteoblasts (ObPm/BPm %), and the number of osteoblasts/mm of bone were analysed. The percentage of bone covered by osteoclasts (OcPm/BPm %), and the number of osteoclasts/mm of bone were determined.

Assessment of bone formation rates using calcein double-labelling

Mice were injected i.p. with 30 mg/kg of calcein 6 d and 2 d prior to sacrifice. Femora were fixed in 70% ethanol, and embedded in LR-white prior to analysis by UV fluorescence microscopy. Mineralization (MS, %) was calculated as $((dL + 0{\cdot}5sL)/BPm) \times 100$ where dL is the double label perimeter, sL is the single label perimeter and BPm is the total bone perimeter. The mineral apposition rate (MAR, μm/d) was calculated as Il.W/number of days between injections, where Il.W is the inter-label width. The bone formation rate (BFR, $mm^2 \times 10^{-3}$/mm/d) was calculated as $(MAR \times (dL + 0{\cdot}5sL))/BPm$.

Colony-forming unit (CFU) assays

Femora were scraped and rinsed in 70% ethanol. After flushing out the marrow plugs, bones were crushed and rinsed extensively to remove remaining attached cells prior to digestion in collagenase (0·25%; Sigma-Aldrich, Gillingham, UK). Cells were washed, plated at 1×10^5 cells/well, and incubated for 2 weeks in Mesencult (Stem Cell Technologies, Cambridge, UK). After rinsing, cultures were fixed with acetone and stained for alkaline phosphatase (ALP) using Napthol AS-MX phosphate (Sigma-Aldrich). Colony-forming units (CFU) containing >50 cells were enumerated by light microscopy.

In vitro *co-culture of pre-osteoblasts with MM cells and cell cycle analysis*

Adult human mesenchymal stem cells (hMSC) were obtained from adult donor bone marrow mononuclear cells by culturing the adherent fraction in Mesencult as detailed previously (Rabin *et al*, 2007). Pre-osteoblasts (pre-OB) were obtained by incubating semi-confluent cultures of hMSC with osteogenic medium as previously described (Kassen *et al*, 2014) for 48 h, before addition of MM cells for co-culture. We used either human myeloma cell lines (HMCL, KMS12BM, KMS12PE, or U266), non-myeloma cell lines (697, SupT1) or freshly isolated $CD138^+$ cells from patient bone marrow aspirates. After 24 h, cells were harvested, and analysed for cell cycle profiles as previously described (Quinn *et al*, 2011) using allopyhcocyanin (APC)-conjugated anti-CD138 mAb (Miltenyi Biotech, Woking, UK) to identify MM cells. Samples were run on a flow cytometer (Cyan ADP, Dako, UK) and analysed using Summit software (Beckman Coulter, High Wycombe, UK).

Real-time PCR analysis

Cells from compact bone and from the marrow plugs were negatively depleted of haemopoietic cells using Ter119 and GlyA MACS magnetic beads, and used for RNA extraction. cDNA was reverse transcribed from 500 ng of total RNA using Superscript II reverse transcriptase (Life Technologies, Paisley, UK). Gene expression was measured on an Eppendorf thermal cycler using a Power Sybr Green Mastermix (Applied Biosystems, Paisley, UK) reaction according to manufacturer Instructions. Primers are shown in the Supporting Information.

Statistics

Data were analysed using GraphPad Prism version 6 (GraphPad Software Inc., La Jolla, CA, USA) and groups were compared using Student's *t*-test, or the Mann–Whitney *U*-test, where appropriate. A *P*-value of <0·05 was considered significant.

Results

Establishing the kinetics of disease progression in KMS12BM xenogenic model

We analysed the kinetics of tumour engraftment in the KMS12BM model. Following tumour cell injection (10^7 luciferase-transduced KMS12BM cells) animals were imaged weekly. By 2 weeks post-injection, low signal intensities were detectable in approximately 50% of the animals, and by

© 2015 John Wiley & Sons Ltd

3 weeks, most animals had low level evidence of disease (Fig 1). Levels increased thereafter, until 8 weeks, when signal intensities were high (Fig 1), and some animals displayed external signs of disease, including ruffled hair and hind limb paralysis. All injected animals developed disease by 8 weeks. Based on these disease kinetics, experiments were designed to assess parameters of bone disease at 1, 3 and 8 weeks post-tumour cell-injection. All animals selected for analysis at 3 weeks had evidence of tumour take by luciferase imaging, and engraftment of KMS12BM cells within the bone marrow was confirmed by immuno-histochemistry using an anti-VS38C antibody (Fig 2). At 1 week, there was no VS38C staining above background in the bone marrow (not shown), however by 3 weeks either single cells (Fig 2C, D arrowed) or small clusters of VS38C-positive cells (Fig 2A, B) were present. At 8 weeks, all femora showed moderate to heavy infiltration with VS38C-positive tumour cells (Fig 2E–H).

Establishing the time frame of bone loss during disease progression

We next investigated the evolution of bone loss in this model, by assessing changes in bone morphology. Femora of animals at 1 week ($N = 24$), 3 weeks ($N = 27$) and 8 weeks ($N = 10$) were analysed by microCT. 3-dimensional reconstruction of femurs revealed the presence of osteolytic lesions

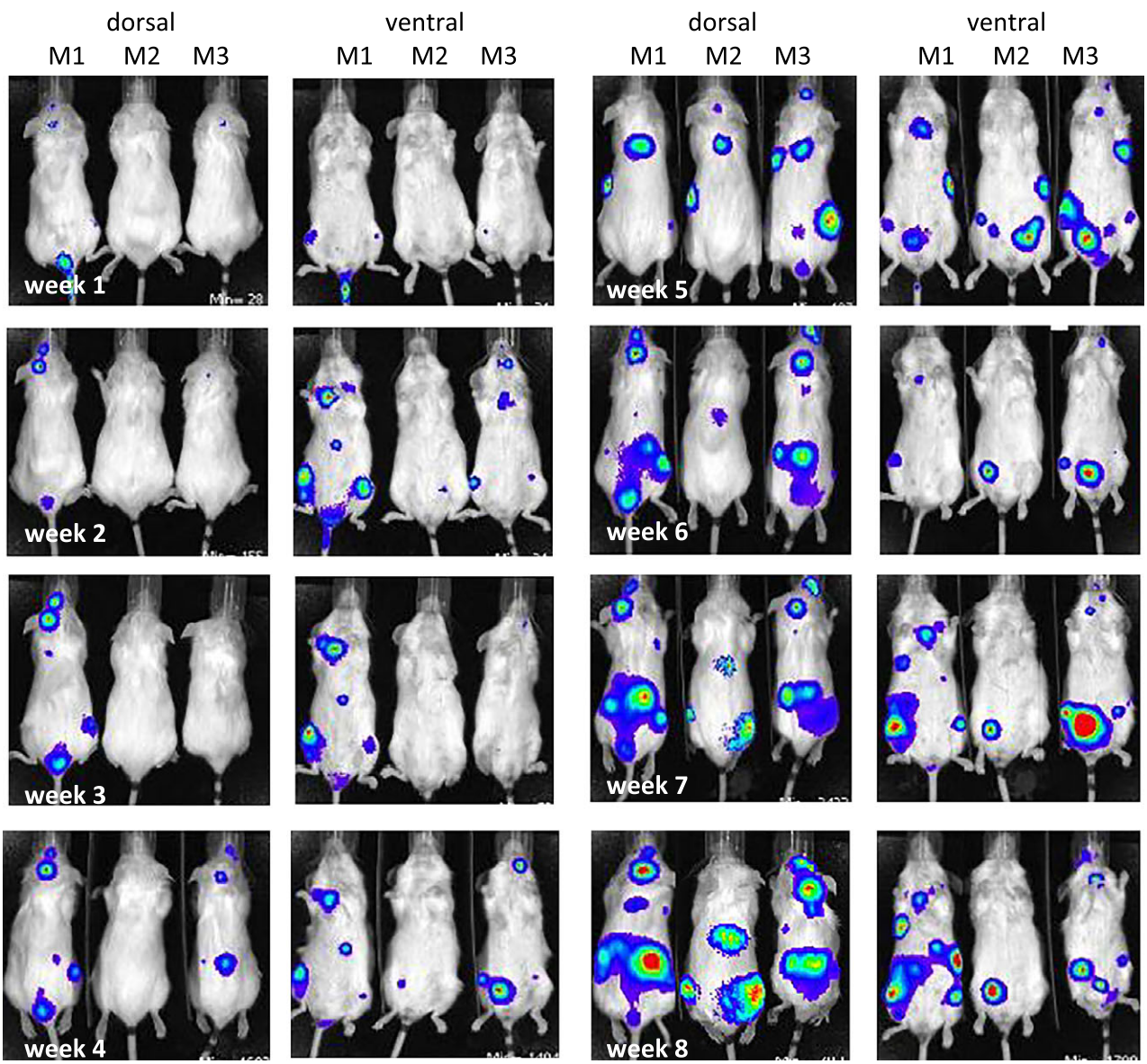

Fig 1. *In vivo* tracking of i.v. injected KMS12BM human myeloma cells. 8-week-old β2m/NOD/SCID animals were transplanted with luciferase tagged KMS12BM cells by tail vein injection (10^7 cells/animal). Disease progression was monitored by live animal imaging over a period of 8 weeks. The same three animals were imaged weekly post-injection.

© 2015 John Wiley & Sons Ltd

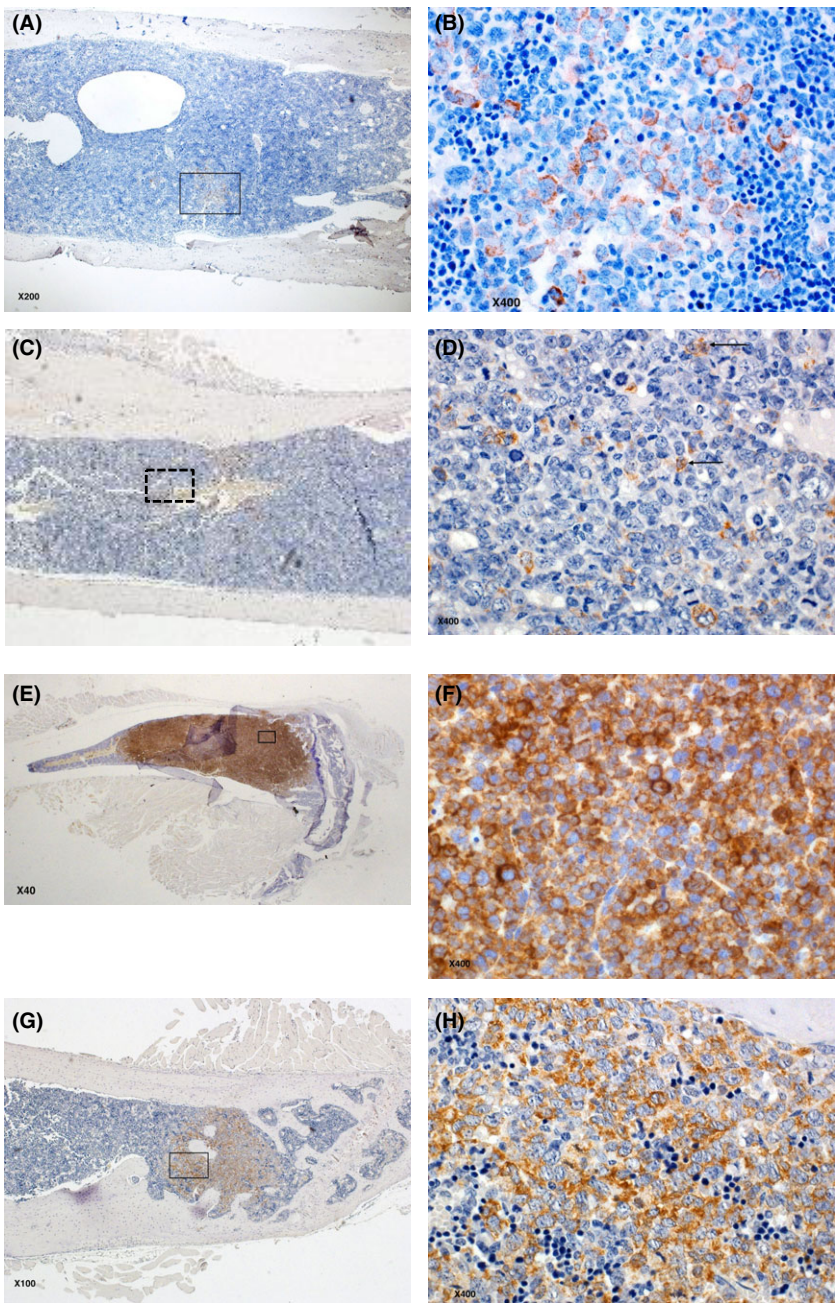

Fig 2. Medullary engraftment of tumour cells. Sections of femora were stained with anti-human VS38C to track medullary localization of myeloma cells at 3 weeks (A–D) and 8 weeks (E–H) post i.v. injection of tumour cells. Each picture on the right is a high power magnification of the area indicated by the black rectangle on the corresponding picture on the left. Magnifications are as indicated on each picture. (A)–(D) are from two representative 3-week diseased animals, showing low level infiltration where the brown-stained tumour cells are seen in clusters (B), or single cells, arrowed in (D). (E)–(H) show heavier infiltration in advanced disease (two representative animals), where tumour almost completely fills the bone in (E) and (F), or is seen as a solid tumour at one end of the bone in (G).

in animals at 8 weeks but not earlier in the disease course (Fig 3A). These pathological lytic lesions are distinct from the small lesions that represent vessel portals in age-matched control animals. The total lesional area in diseased animals was greater compared with control animals at 8 weeks ($P = 0{\cdot}05$, Fig S2). Parametric analysis using microCT, however, revealed significant reduction in BV as early as 3 weeks in diseased animals (control, $11{\cdot}4 \pm 3{\cdot}7\%$, cf. diseased, $10{\cdot}3 \pm 3{\cdot}1\%$, $P = 0{\cdot}017$, Fig 3B). As expected, BV in diseased animals was also decreased at 8 weeks (control, $8{\cdot}3 \pm 1{\cdot}4\%$, cf. diseased, $6{\cdot}1 \pm 2{\cdot}6\%$ $P = 0{\cdot}04$), as was trabecular number (control, $1{\cdot}89 \pm 0{\cdot}46$/mm, cf. diseased, $1{\cdot}36 \pm 0{\cdot}50$/mm, $P = 0{\cdot}03$, Fig 3C). At all time points, control and experimental animals were age-matched.

Changes in osteoclast and osteoblast numbers occur late in the disease process

Next, we examined the timeframe of changes in osteoclasts and osteoblasts, by static histomorphometry. We observed no significant differences between control and diseased groups at early stages of disease. At 1 and 3 weeks post-injection of tumour cells, few osteoclasts were present at the endocortical surface of the bone, with little difference between control

© 2015 John Wiley & Sons Ltd

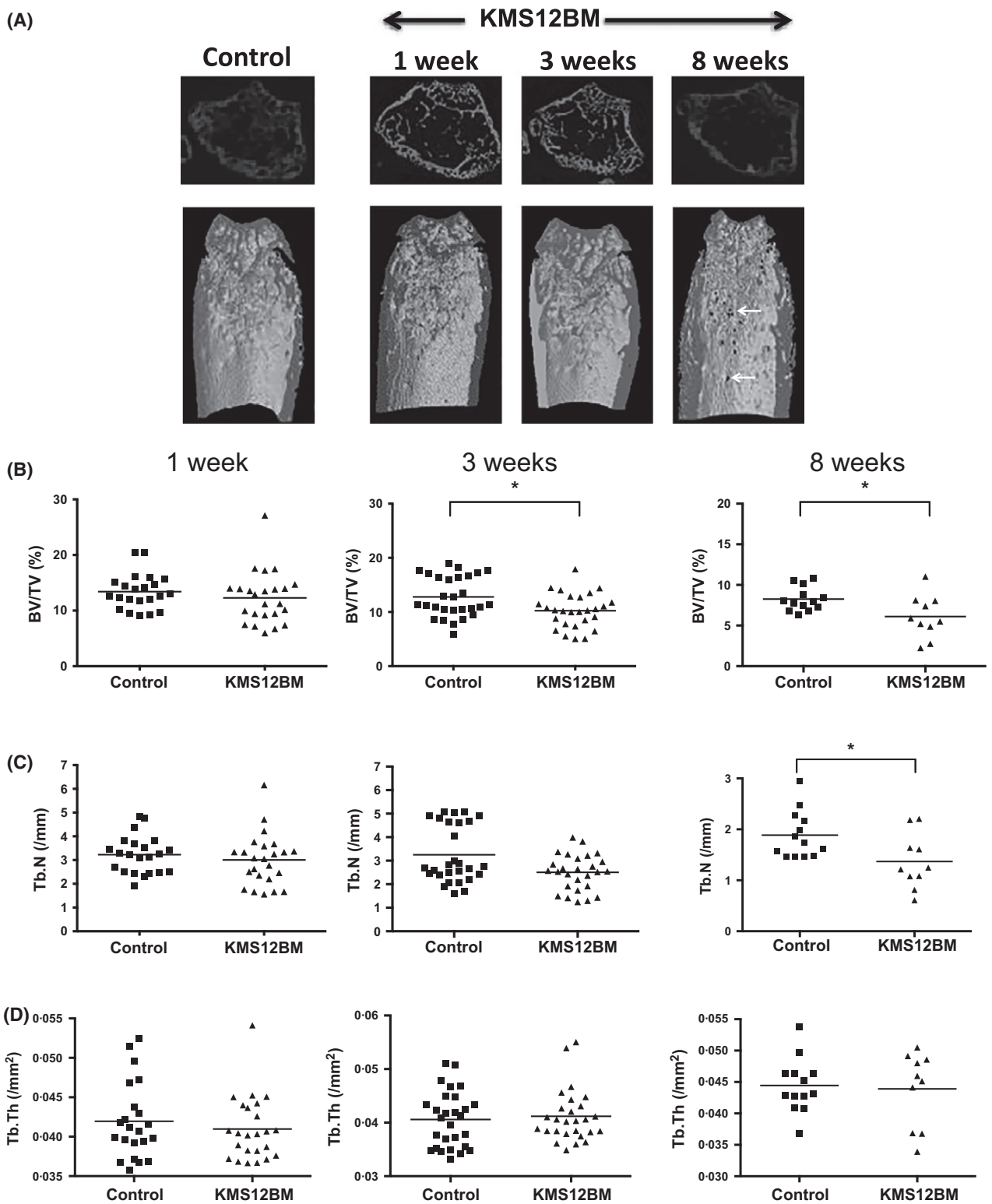

Fig 3. Micro-computerized tomography analysis of femora from control and diseased (KMS12BM) animals at 1, 3 and 8 weeks. (A) 3D reconstruction and 2D cross sections of control and diseased femora from representative animals. Osteolytic lesions are seen at 8 weeks (arrowed), but not before. Bone volume (B), trabecular number (C) and trabecular thickness (D) are shown for animals at 1, 3 and 8 weeks. Data for individual animals shown, with median values indicated. $*P < 0{\cdot}05$, $**P < 0{\cdot}01$.

© 2015 John Wiley & Sons Ltd

and diseased animals (Fig 4 A-C) At these time points, osteoblast parameters were also similar between the two groups (Fig 4B, C). The most notable changes were seen at 8 weeks at the endocortical surface, where there was an increase in osteoclast numbers (control, 0·73 ± 0·8/mm, cf. diseased, 2·89 ± 2·1/mm, $P = 0·05$) and in endocortical area covered by osteoclasts (control, 2·44 ± 3·0%, cf. diseased, 6·17 ± 5·0%, Fig 4D). A striking decrease in osteoblast number was also observed at 8 weeks (control, 7·38 ± 3·3/mm, cf. diseased, 2·53 ± 2·9/mm, $P = 0·007$) with a corresponding decrease in the endocortical surface utilized (control, 12·62 ± 6·0%, cf. diseased, 3·58 ± 4·4%, $P = 0·005$, Fig 4D). Changes in osteoclast and osteoblast numbers and perimeter therefore occur late in disease course, thus are unlikely to account for the earlier structural changes observed at 3 weeks in diseased animals (Fig 3B). Osteoclast and osteoblast numbers and perimeter on trabecular surfaces showed little change (Fig S3).

Bone formation rates are reduced at an early stage of disease development

This led us to examine functional changes with dynamic histomorphometry and calcein labelling. At 1 week post-tumour cell injection, there were no differences between injected or control animals at either the trabecular or cortical surfaces ($n = 8$, Fig 5A–D). By 3 weeks, reduction in the distance between labelled surfaces is seen in diseased animals, indicat-

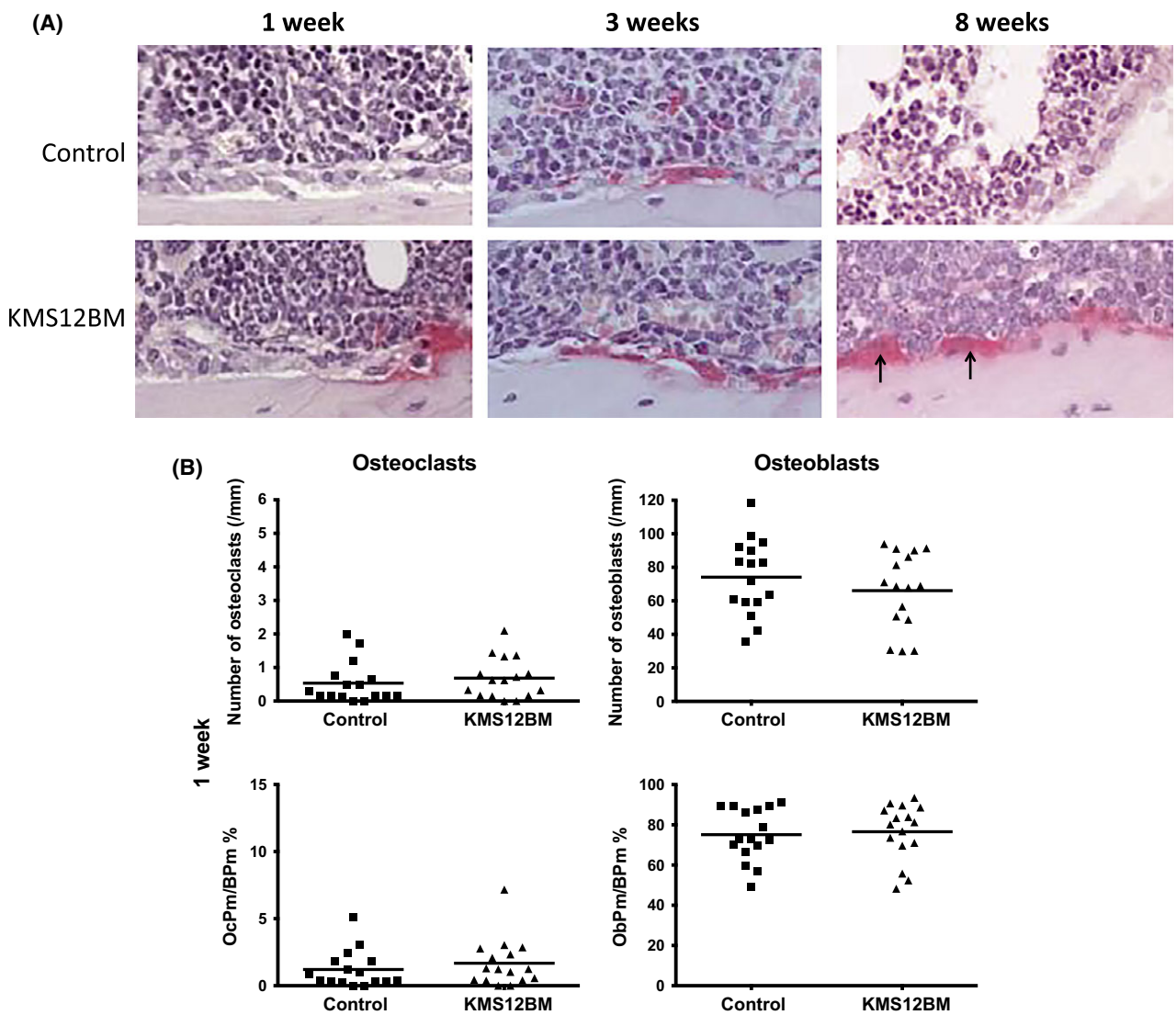

Fig 4. Changes in osteoblast and osteoclast numbers in diseased (KMS12BM) animals, assessed using static histomorphometry (A) TRAP stain of cortico-endosteal femoral sections reveal an increase in osteoclasts (arrowed) in diseased animals at 8 weeks. (B) Osteoclast (left panels) and osteoblast (right panels) numbers and perimeter at 1 week (C) 3 weeks, and (D) 8 weeks. Data for individual animals shown, with median values indicated. $*P < 0·05$, $**P < 0·01$.

© 2015 John Wiley & Sons Ltd

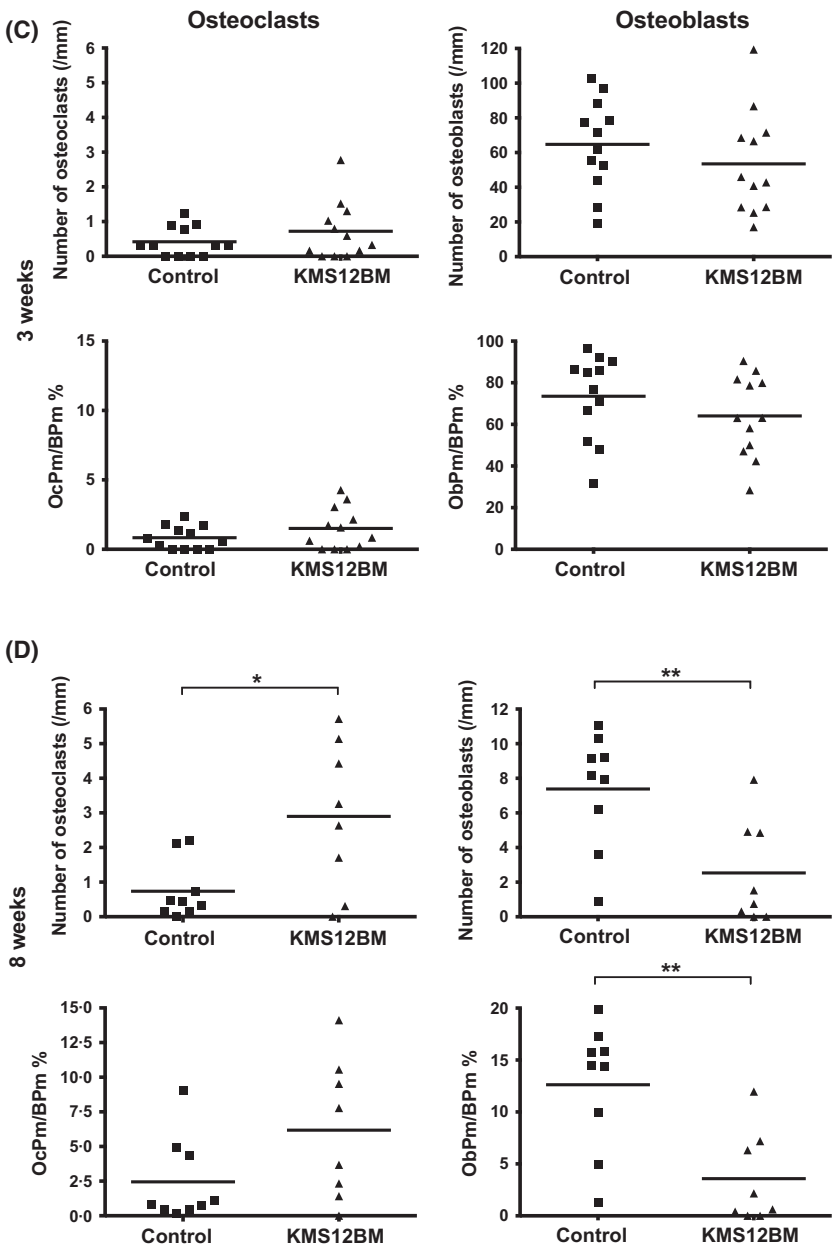

Fig 4. Continued

ing reduced bone formation (Fig 5A). At this stage, diseased animals displayed reduced mineral apposition rate (control, 2·88 ± 0·66 μ/d, cf. diseased, 1·99 ± 0·76 μ/d, $P = 0·004$) and bone formation rate (control, 2·38 ± 0·81 $mm^2 \times 10^{-3}$ μ/m/d, cf. diseased, 1·68 ± 0·41 $mm^2 \times 10^{-3}$ μ/m/d, $P = 0·04$) in cortical bone (Fig 5B, D). Mineralization of trabecular surfaces at 3 weeks was also significantly lower than in control animals (control, 23·77 ± 7·6%, cf. diseased, 16·68 ± 7·4%, $P = 0·02$, Fig 5C). As expected, mineralized surface was significantly lower in diseased animals by 8 weeks (control, 60·17 ± 7·1%, cf. diseased, 38·55 ± 15·0%, $P = 0·02$) (Fig 5C). The reduction in mature osteoblast function at 3 weeks of disease development probably accounts for the structural changes seen in Fig 3B, and suggests that although osteoblasts are present at 3 weeks, they may not be functionally competent.

Early disease establishment is associated with an increase in bone CFU

Next we examined the osteo-progenitor compartment, using CFU assays on 'bone lining cells', obtained from the endo-cortical bone surface, which may be a rich source of osteo-progenitors. These 'bone lining cells' were incubated for 2 weeks in Mesencult media without osteoblast differentiation factors before staining for alkaline phophatase (ALP). Several types of

© 2015 John Wiley & Sons Ltd

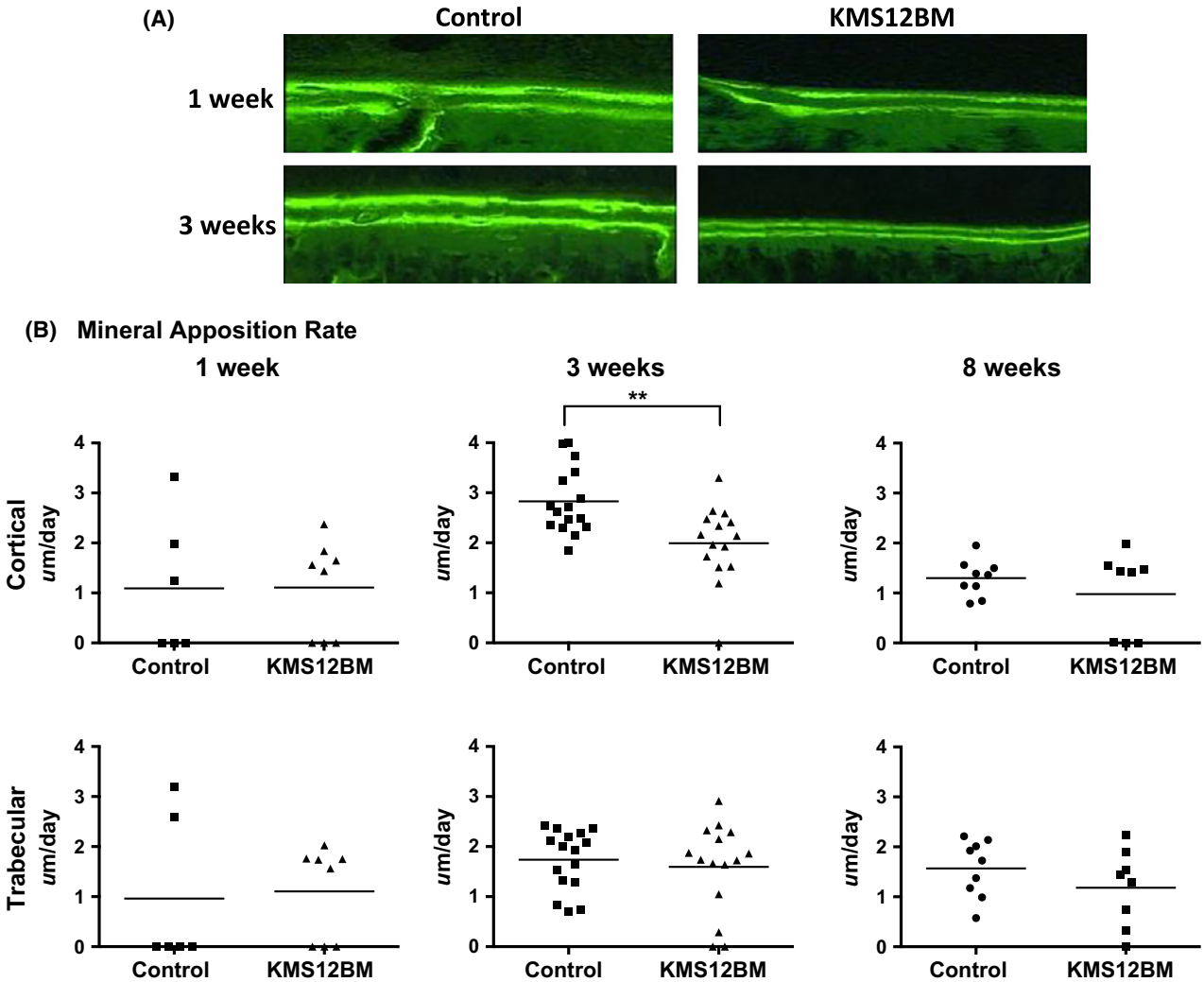

Fig 5. Dynamic histomorphometry to assess bone formation rates. This was performed on femora, by analysis of calcein labelling. (A) UV fluorescence microscopy shows the distance between labelled cortical bone surfaces at 1 and 3 weeks, a greater distance is indicative of higher rate of bone formation. Mineral apposition rates (B), mineralization surface (C) and bone formation rates (D) in control and diseased (KMS12BM) animals at cortical and trabecular surfaces are shown at each time point. Data for individual animals shown, with median values indicated. $^{*}P < 0{\cdot}05$, $^{**}P < 0{\cdot}01$.

colonies were observed (Fig S4A) but the majority were osteoprogenitors, i.e., ALP^{+}. CFU derived from diseased animals at 1 week ($N = 12$), 3 weeks ($N = 12$) and 8 weeks ($N = 9$) post-tumour cell injection were quantified and compared to age-matched, non-injected control animals. Notably, there was a significant increase in ALP^{+} CFUs as well as the total number of CFUs at 1 week (control, $49{\cdot}8 \pm 12{\cdot}1/10^{5}$ cells, cf. diseased $72{\cdot}4 \pm 24$, $P < 0{\cdot}01$, Fig 6A, B). The proportion of ALP^{+} colonies was similar in both groups (Fig S4B). By 3 weeks, total CFU and ALP^{+} CFU from diseased animals were reduced compared to control animals ($P < 0{\cdot}05$, Fig 6A, B). There was also a significant reduction in proportion of ALP^{+} CFU at this time point ($P < 0{\cdot}01$, Fig S4B), suggesting that the defect is more pronounced in the pre-osteoblast progenitor compartment. By 8 weeks, CFU numbers were lower in both control and diseased animals, in keeping with the older age of these animals, however, diseased animals demonstrated a marked reduction in these stromal progenitors when compared to control animals ($P < 0{\cdot}001$ for both total and ALP^{+} CFU, Fig 6B). These data suggest that the osteo-progenitor population in myelomatous bone undergoes changes at a very early stage of disease, with an initial increase followed by a steady decline.

Myeloma cells induce cell cycling in pre-osteoblasts

To explore the mechanisms underlying the early increase in osteoprogenitors in diseased bones, we set up *in vitro* co-culture experments using pre-osteoblast cultures derived from adult human MSC. Cell cycle analysis was performed as previously described (Quinn *et al* 2011). When semi-confluent pre-osteoblast cultures were incubated with MM cells for 24 h, there was a significant increase in the

© 2015 John Wiley & Sons Ltd

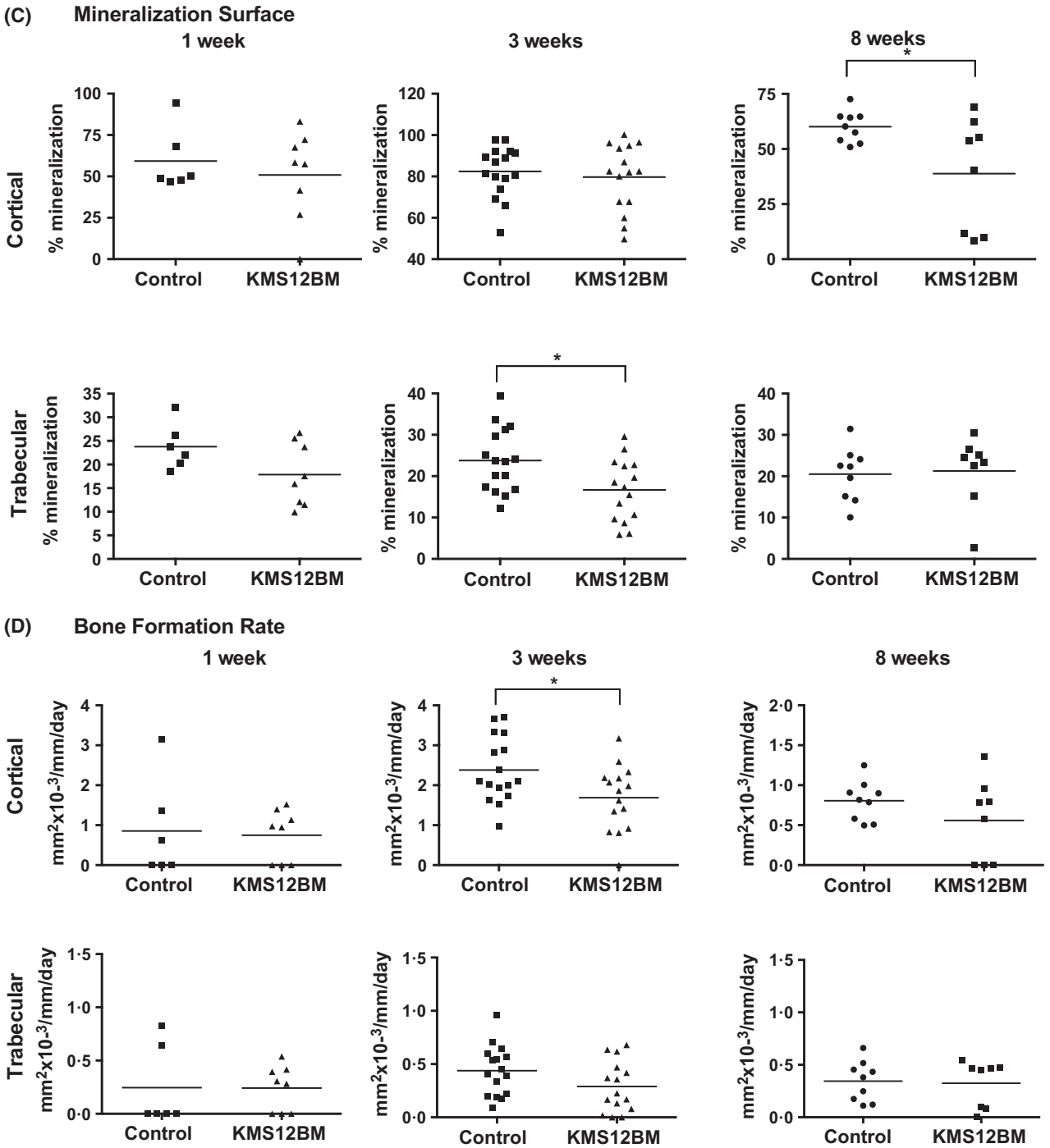

Fig 5. Continued

fraction of pre-OB cells in the proliferative phase of the cell cycle (S+G2/M, Fig 6C). This effect was seen with the MM cell lines KMS12BM and KMS12PE, but not with the non-MM cell lines (697 and SupT1). We observed a similar effect in one experiment using primary CD138^{+} MM cells (Fig 5SA). We also observed a dose dependent effect using the MM cell line H929 (Fig S5B). These observations suggest that the initial encounter with MM cells causes cellular proliferation in pre-osteoblastic stromal cells in the bone marrow.

Temporal changes in gene expression in the stromal compartment

Next we examined the expression levels of several genes considered to play roles in tumour growth and bone disease,

© 2015 John Wiley & Sons Ltd

comparing diseased and control animals at 3 and 8 weeks. We assessed these genes in the stromal and osteoprogenitor compartment, depleted of haemopoietic cells. We observed time-dependent changes in expression of several cytokine, chemokine and angiogenic genes as well as some implicated in osteoclastogenesis and osteoblast suppression. Changes in expression for each gene were analysed with respect to age-matched control animals; in order to display the changes over time, the controls have been grouped, as there was no significant difference between 3- and 8-week control animals for any of the genes studied. Early in disease course (3 weeks) there was a significant increase in CCL3 (MIP-1α), a chemokine that has been implicated as a growth and survival factor for MM tumour cells, as well as an osteoclastogenic factor (Han *et al*, 2001; Oyajobi *et al*, 2003) but levels fall by 8 weeks (Fig 7). There is also an increase in IL6, an established MM growth factor, at 3 weeks, although it does not reach significance in this series of animals. Notably, IL6, IL6R, BAFF (TNFSF13B) and VEGF (VEGFA) are all significantly reduced at 8 weeks of disease, suggesting that these stromal-derived MM growth factors are no longer critical for tumour growth/survival at this late stage. The osteoclastogenic factor, RANKL (TNFSF11), is significantly increased only at 8 weeks, as is the WNT antagonist, DKK1. Reduced expression of the adhesion molecules VLA4 (ITGA4), LFA1 (ITGB1) and VCAM1 at 8 weeks probably signifies profound changes in the stromal compartment, that accompany advanced disease. Figure S6 shows the expression of each gene relative to the age-matched controls at each time point.

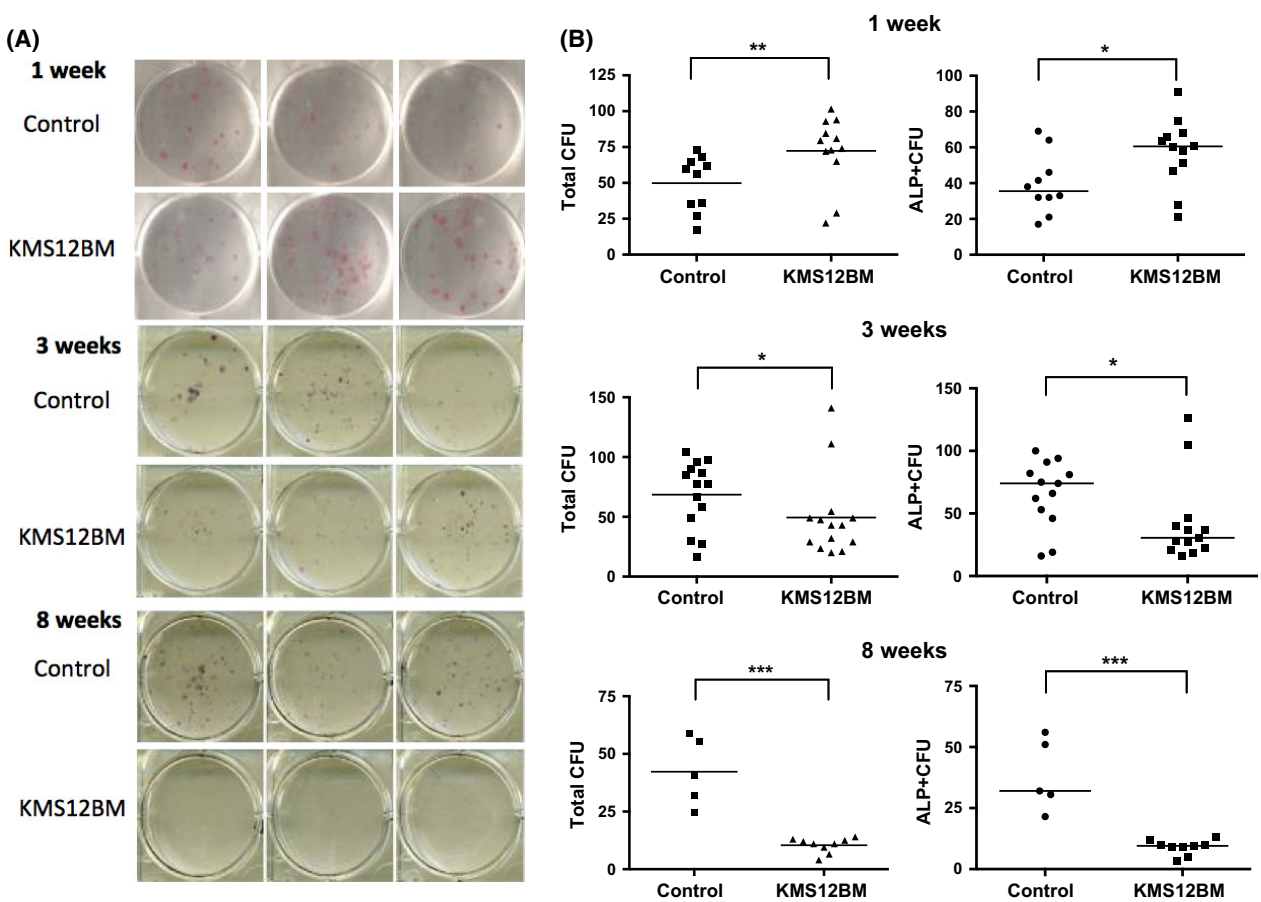

Fig 6. CFU content in bone lining cells obtained from control and diseased animals. Femoral bones were crushed and digested with collagenase after removal of marrow plugs. Cells obtained were plated in duplicate in Mesencult medium and incubated for 2 weeks prior to staining for ALP. (A) Representative stained cultures from control and diseased (KMS12BM) animals at 1, 3 and 8 weeks, three animals each. (B) Total and ALP+ colonies at 1, 3 and 8 weeks. Data for individual animals shown, with median values indicated. $*P < 0{\cdot}05$, $**P < 0{\cdot}01$, $***P < 0{\cdot}001$. (C) (D) Effect of MM cells on cell cycle profiles in adult human MSC-derived pre-osteoblasts. Semi-confluent pre-osteoblasts were co-cultured with MM cell lines (KMS12BM, KMS12PE) or non-MM cell lines (697, SupT1) for 24 h. Cultures were then harvested and analysed for cell cycle profiles, gating on the pre-osteoblast population. (C) shows representative flow cytometric plots from one experiment with percentage cells in S+G2/M indicated. while (D) summarizes the results of five experiments, each with a different MSC donor. Data are presented as box and whisker plots, $**P < 0{\cdot}01$, $***P < 0{\cdot}001$ compared to control (pre- osteoblast cultured alone). CFU, colony-forming unit; ALP, alkaline phosphatase; MM, multiple myeloma; MSC, mesenchymal stem cells.

© 2015 John Wiley & Sons Ltd

Discussion

The KMS12BM model recapitulates human MM bone disease, with changes in osteoclast and osteoblast numbers and function, BV loss and osteolytic lesions in diseased animals. This model is further validated by the demonstration that bone destruction is reversed by manipulation of the RANKL-OPG axis, using OPG-modified mesenchymal stem cells (Rabin *et al*, 2007). We took advantage of this model, using luciferase-modified MM cells to track the kinetics of disease development, and compared early with late diseased animals, to investigate the temporal changes in bone physiology that result ultimately in osteolytic lesions. We observed functional changes in the mature osteoblast compartment at an early stage of disease when tumour infiltration is low (3 weeks) and osteolytic lesions are not yet present. At this time, there were significant reductions in BV, bone formation rates and osteo-progenitor content of bone lining cells, despite normal (compared to age-matched control animals) osteoclast and osteoblast numbers at trabecular and cortical surfaces. On the other hand, we observed a striking expansion of the osteo-progenitor compartment at 1 week, when MM tumours have barely established in the bones; this is reversed by 3 weeks, continuing to decrease thereafter. Finally we report time-dependent changes in expression of genes related to tumour growth, cell migration and bone metabolism in the stromal/pre-osteoblast compartment.

Multiple myeloma cells establish intimate spatial relationships with bone cells and are hence likely to exert effects soon after their arrival in the bone marrow. We document one such effect in the early (at 1 week) increase in osteo-progenitor numbers in bone-lining cells of compact bone. Intriguingly, this effect is rapidly reversed after 2 weeks. Our observation is reminiscent of earlier reports of increased osteoblast recruitment in early disease stage of MM (Bataille *et al*, 1991). The initial expansion in the stromal compartment is also in keeping with a recent report of an increase in nestin+ mesenchymal cells in the femoral bone marrow of NOG mice engrafted with MM cells (Iriuchishima *et al*, 2012). Our *in vitro* observation that MM cells induce increased cell cycling in pre-osteoblasts, and also in MSC (Kassen *et al*, 2014) suggest one explanation for these findings. We have also previously reported that MM cells directly increase osteoblast recruitment via an sIL6R dependent mechanism (Karadag *et al*, 2000), while Noll *et al* (2014) observed an increase in MSC numbers following tumour inoculation in the C57BL/KaLwRij murine myeloma model. A recent study also supports the notion that MM cells induce

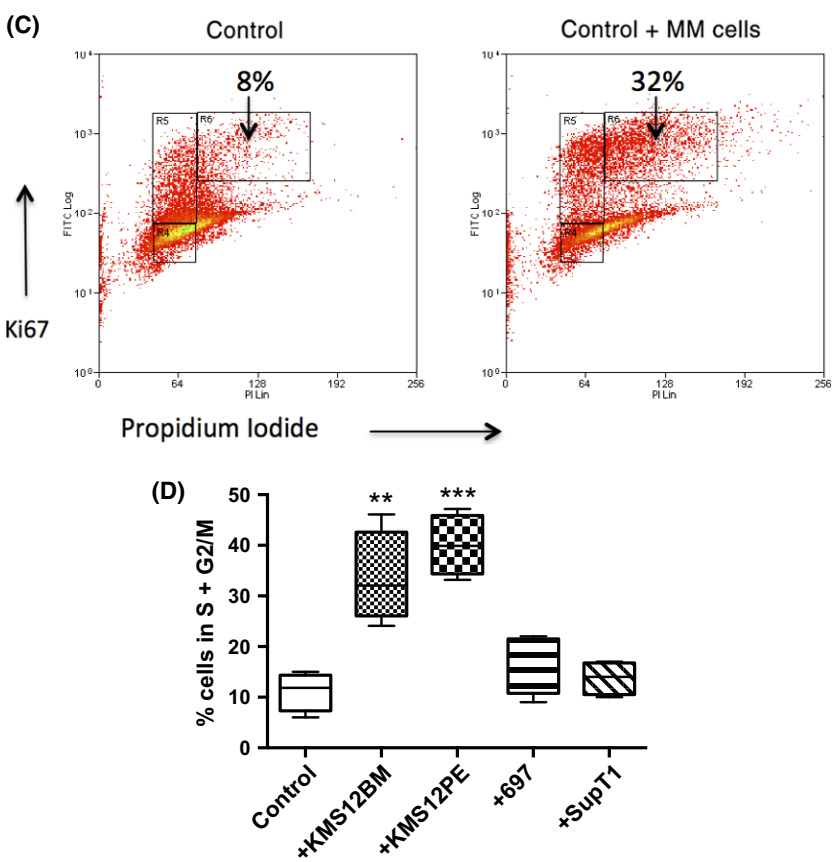

Fig 6. Continued.

© 2015 John Wiley & Sons Ltd

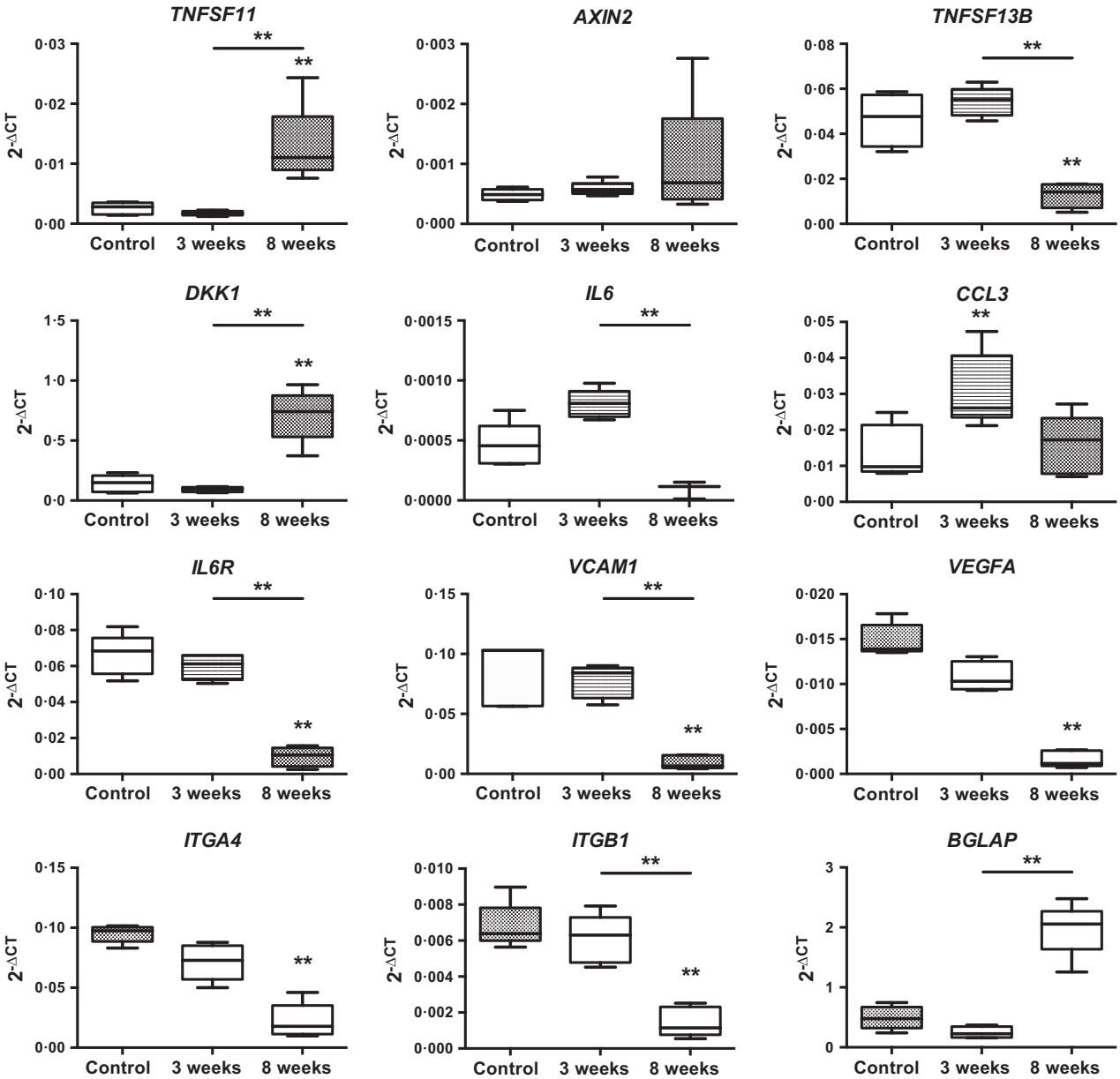

Fig 7. Expression of selected genes in the stromal compartment of control and diseased animals. Bone lining cells and marrow plugs were depleted of haemopoietic cells before being subjected to quantitative polymerase chain reaction. Gene expression was analysed at 3 and 8 weeks post-tumour cell injection. Results are normalized to the housekeeping gene *Hsp90ab1* and $2^{-\Delta CT}$ values are shown. Data are presented as box and whisker plots, $*P < 0{\cdot}05$, $**P < 0{\cdot}01$ compared with control, where significant differences exist between 3- and 8-week diseased animals, these are indicated by a horizontal line and the *P*-value.

proliferation in fibroblastic cells (Frassanito *et al*, 2014). Such cellular changes may be integral to the establishment of an early MM niche in which osteoblasts play a role, as suggested by a study on the localization of dye-labelled quiescent MM cells in a similar xenogeneic model (Chen *et al*, 2014). The loss of osteoblast numbers and function later in disease course may reflect tumour evolution to reduced dependence on osteoblast-derived factors and/or an increase in compensatory growth factors released by on-going bone resorption, e.g IGF-I (Sprynski *et al*, 2009).

Despite the fact that osteoblast numbers (and perimeter) are preserved until 8 weeks, bone formation rates, assessed by calcein labelling, and BV, assessed by microCT, are already reduced at 3 weeks, suggesting that the key changes at this stage are functional in nature. Perturbations in bone formation may also reflect alterations in the progenitor compartment, hence we obtained bone lining cells, that are reported to be a richer source of CFU when compared to the marrow plug (Short *et al*, 2009). These cells were set up in colony assays *without* osteoblast differentiation stimuli, hence

© 2015 John Wiley & Sons Ltd

the ALP$^+$ colonies reflect osteoblast progenitors. Interestingly, both total CFU as well as the percentage of ALP$^+$ CFU fall from 3 weeks onward, suggesting a more profound effect on the osteo-progenitors. The striking fall in ALP$^+$ CFU at 3 weeks may account for the reduction in mature OB at 8 weeks, when overt bone loss is the result of both reduced osteoblast numbers and impaired function. Our observations on the early changes in dynamic bone formation and osteo-progenitor numbers when tumour burden is low provide a compelling rationale for clinical intervention at an early stage of disease, when patients are still relatively asymptomatic and support the recent change in recommendations regarding treatment of high risk smouldering myeloma (Rajkumar *et al*, 2014). Several groups have reported abnormal bone metabolism in asymptomatic myeloma or MGUS, reinforcing the concept that, even while the tumour is in its pre-malignant phase, bone physiology is already affected (Laroche *et al*, 1996; Vejlgaard *et al*, 1997; Woitge *et al*, 2001). The timing of the observed changes cannot simply be related to tumour burden because many patients experience widespread lytic disease with relatively low tumour burden, and recent reports suggest that magnetic resonance imaging (MRI)-defined lesions are an independent risk factor for progression from smouldering to symptomatic MM (Hillengass *et al*, 2010; Kastritis *et al*, 2014).

To gain an understanding of the mechanisms underlying the early changes in the bone environment in this model, we investigated the expression of genes considered to feature in tumour growth (*IL6*, *IL6R*, *TNFSF13B*, *VEGFA*, *CCL3*), in osteoclast activation (*TNFSF11*, *CCL3*), angiogenesis (*VEGFA*), osteoblast suppression (*DKK1*), osteoblast differentiation and function (*AXIN2*, *BGLAP*) and cell adhesion (*ITGB2*, *VCAM1*). We observed that both *TNFSF11* and *DKK1* were not increased until 8 weeks, while CCL3 is initially elevated at 3 weeks, but falls thereafter. *CCL3* is a pro-inflammatory cytokine that belongs to the CC chemokine family and plays a role in recruitment and differentiation of osteoclast precursors (Han *et al*, 2001); it is upregulated in MM bone marrow, and is chemotactic for both MM cells and osteoclasts (Lentzsch *et al*, 2003; Uneda *et al*, 2003), thus serving to promote tumour progression as well as bone lysis. Osteoblasts also express CCL3 receptors, and recent work in the human system suggests that while CCL3 has no effect on osteoblast differentiation, it impairs osteoblast function as assessed by matrix mineralization and the production of osteocalcin (Vallet *et al*, 2011). Thus, the elevated levels of CCL3 at 3 weeks provide an explanation for the reduction in mature cell function at this time, despite preserved osteoblast numbers. Late in disease evolution (8 weeks), osteoblast suppression reflects both reduced differentiation and impaired function, and the rise in DKK1 levels suggest that disruption of WNT signalling may play a role at this stage. At this time, the fall in CCL3 levels may relate to the profound loss of osteoblast numbers, as these cells are a source of CCL3 in the bone marrow (Laroche *et al*, 1996). The early rise in CCL3, followed by late rise in RANKL at 8 weeks, may also give clues to the time-dependent mechanisms involved in osteoclastogenesis, with CCL3 perhaps functioning to recruit osteoclast progenitors early on in the disease process, while RANKL acts to increase differentiation and activation at later stages. IL6 and BAFF (TNFSF13B) are growth and survival factors for MM cells, and the trend to increased levels at 3 weeks probably relates to tumour growth. Levels of several stromal-derived MM growth/survival factors (BAFF [TNFSF13B], IL6, IL6R, VEGFA) fall at 8 weeks, perhaps reflecting the profound disturbance of stromal physiology at this later disease stage, when other factors, e.g., matrix bound proteins released during bone resorption, become important. The late (8 weeks) rise in OCN (BGLAP) and AXIN (AXIN2) are unexpected, as osteoblast numbers and function are reduced at this time, but this may simply reflect the stage of differentiation of the cells, with consequences for osteoclast regulation. AXIN, for example, is a negative regulator of the WNT pathway, and increased levels in osteoprogenitor/stromal cells may promote RANKL (TNFSF11) production and hence osteoclastogenesis (Yan *et al*, 2009). OCN (GLAP) expression is suppressed by CCL3, which may explain the lower levels at 3 weeks, and subsequent rise at 8 weeks. The consistent downregulation of the adhesion molecules LFA-1 (ITGB2), VLA-4 (ITGA4) and VCAM1 at 8 weeks may reflect the reduced dependence of tumour cells on adhesive interactions in advanced disease, but may also have implications for osteoblast function.

In summary, we describe temporal changes in bone physiology using the KMS12BM medullary model of MM bone disease. Our findings indicate that the arrival of MM cells in the bone marrow has distinct effects on two cellular compartments responsible for bone formation. Firstly, we observe that functional changes in mature osteoblasts occur early (3 weeks), prior to quantitative reduction in these cells, and the appearance of lytic lesions (8 weeks). Secondly, an even earlier effect on the osteo-progenitor compartment can be seen (at 1 week), in the form of a proliferative stimulus, indicative of an initial expansion of these cells. Later in the disease course, this compartment declines rapidly, leading to depletion of mature bone forming cells that is seen on static histomorphometry at 8 weeks. We also report time-related changes in gene expression in the stromal and pre-osteoblast compartment, providing mechanistic clues. An important clinical implication of our findings is that interventions to halt osteoblast suppression should be considered at an early stage in disease development. This is consistent with the recent revision of the International Myeloma Working Group definition of symptomatic myeloma, to include patients with bone lesions on MRI, who are otherwise asymptomatic (Rajkumar *et al*, 2014), and support the development of more refined tools to detect these early changes in bone physiology in asymptomatic precursor disease. Such tools should ideally distinguish otherwise asymptomatic patients who are at risk

© 2015 John Wiley & Sons Ltd

of developing osteolysis even when tumour burden is low. Our findings lend support for the development of strategies for early intervention to prevent the changes in bone physiology that lead ultimately to osteolytic bone destruction.

Authorship

KY was the principal investigator and takes primary responsibility for the paper. DK, DL, AL and HE performed the work, KY, PC, NR and DK designed the studies, KY, DK and AC analysed the data, KY, DK and PC wrote the paper. All authors have read the paper and approve of its contents.

Acknowledgements

This work was supported by grants from Cancer Research UK (DK) and Leukemia and Lymphoma Research (AC, DL, HE). The work was undertaken at University College London/University College London Hospitals, which is an NIHR Biomedical Research Centre, a CRUK Cancer Centre and a Leukaemia and Lymphoma Research Centre of Excellence.

Conflict of interest

The authors declare no conflict of interest.

Supporting Information

Additional Supporting Information may be found in the online version of this article:

Fig S1. Luciferase modified KMS12BM cell line.

Fig S2. Quantitative analysis of lesions in diseased (KMS12BM) animals and age-matched controls.

Fig S3. Trabecular osteoclast and osteoblast numbers.

Fig S4. Alkaline phosphatase (ALP) expressing CFU from compact bone in control and diseased animals.

Fig S5. Effect of myeloma cells on cell cycle behaviour in pre-ostoblast cells.

Fig S6. Gene expression ($2^{-\Delta CT}$) as fold change compared to control samples at respective time points.

Table SI. Primers used for qPCR.

References

Bataille, R., Chappard, D., Marcelli, C., Dessauw, P., Baldet, P., Sany, J. & Alexandre, C. (1991) Recruitment of new osteoblasts and osteoclasts is the earliest critical event in the pathogenesis of human multiple myeloma. *Journal of Clinical Investigation*, **88**, 62–66.

Bataille, R., Chappard, D. & Basle, M. (1995) Excessive bone resorption in human plasmacytomas: direct induction by tumour cells in vivo. *British Journal of Haematology*, **90**, 721–724.

Bataille, R., Chappard, D. & Basle, M.F. (1996) Quantifiable excess of bone resorption in monoclonal gammopathy is an early symptom of malignancy: a prospective study of 87 bone biopsies. *Blood*, **87**, 4762–4769.

Bolzoni, M., Donofrio, G., Storti, P., Guasco, D., Toscani, D., Lazzaretti, M., Bonomini, S., Agnelli, L., Capocefalo, A., Dalla Palma, B., Neri, A., Nicolini, F., Lisignoli, G., Russo, F., Colla, S., Aversa, F. & Giuliani, N. (2013) Myeloma cells inhibit non-canonical wnt co-receptor ror2 expression in human bone marrow osteoprogenitor cells: effect of wnt5a/ror2 pathway activation on the osteogenic differentiation impairment induced by myeloma cells. *Leukemia*, **27**, 451–463.

Chen, Z., Orlowski, R.Z., Wang, M., Kwak, L. & McCarty, N. (2014) Osteoblastic niche supports the growth of quiescent multiple myeloma cells. *Blood*, **123**, 2204–2208.

Frassanito, M.A., Rao, L., Moschetta, M., Ria, R., Di Marzo, L., De Luisi, A., Racanelli, V., Catacchio, I., Berardi, S., Basile, A., Menu, E., Ruggieri, S., Nico, B., Ribatti, D., Fumarulo, R., Dammacco, F., Vanderkerken, K. & Vacca, A. (2014) Bone marrow fibroblasts parallel multiple myeloma progression in patients and mice: in vitro and in vivo studies. *Leukemia*, **28**, 904–916.

Giuliani, N., Colla, S. & Rizzoli, V. (2004) New insight in the mechanism of osteoclast activation and formation in multiple myeloma: focus on the receptor activator of NF-kappaB ligand (RANKL). *Experimental Hematology*, **32**, 685–691.

Han, J.H., Choi, S.J., Kurihara, N., Koide, M., Oba, Y. & Roodman, G.D. (2001) Macrophage inflammatory protein-1alpha is an osteoclastogenic factor in myeloma that is independent of receptor activator of nuclear factor kappaB ligand. *Blood*, **97**, 3349–3353.

Heino, T.J. & Hentunen, T.A. (2008) Differentiation of osteoblasts and osteocytes from mesenchymal stem cells. *Current Stem Cell Research & Therapy*, **3**, 131–145.

Hillengass, J., Fechtner, K., Weber, M.-A., Bäuerle, T., Ayyaz, S., Heiss, C., Hielscher, T., Moehler, T.M., Egerer, G., Neben, K., Ho, A.D., Kauczor, H.U., Delorme, S. & Goldschmidt, H. (2010) Prognostic significance of focal lesions in whole-body magnetic resonance imaging in patients with asymptomatic multiple myeloma. *Journal of Clinical Oncolology*, **28**, 1606–1610.

Iriuchishima, H., Takubo, K., Miyakawa, Y., Nakamura-Ishizu, A., Miyauchi, Y., Fujita, N., Miyamoto, K., Miyamoto, T., Ikeda, E., Kizaki, M., Nojima, Y. & Suda, T. (2012) Neovascular niche for human myeloma cells in immunodeficient mouse bone. *PLoS One*, **7**, e30557.

Jakob, C., Zavrski, I., Heider, U., Brux, B., Eucker, J., Langelotz, C., Sinha, P., Possinger, K. & Sezer, O. (2002) Bone resorption parameters [carboxy-terminal telopeptide of type-I collagen (ICTP), amino-terminal collagen type-I telopeptide (NTx), and deoxypyridinoline (Dpd)] in MGUS and multiple myeloma. *European Journal of Haematolology*, **69**, 37–42.

Karadag, A., Scutt, A.M. & Croucher, P.I. (2000) Human myeloma cells promote the recruitment of osteoblast precursors: mediation by interleukin-6 and soluble interleukin-6 receptor. *Journal of Bone Mineral Research*, **15**, 1935–1943.

Kassen, D., Moore, S., Percy, L., Herledan, G., Bounds, D., Rodriguez-Justo, M., Croucher, P. & Yong, K. (2014) The bone marrow stromal compartment in multiple myeloma patients retains capability for osteogenic differentiation in vitro: defining the stromal defect in myeloma. *British Journal of Haematology*, **167**, 194–206.

Kastritis, E., Moulopoulos, L.A., Terpos, E., Koutoulidis, V. & Dimopoulos, M.A. (2014) The prognostic importance of the presence of more than one focal lesion in spine MRI of patients with asymptomatic (smoldering) multiple myeloma. *Leukemia*, **28**, 2402–2403.

Laroche, M., Attal, M. & Dromer, C. (1996) Bone remodelling in monoclonal gammopathies of uncertain significance, symptomatic and non-symptomatic myeloma. *Clinical Rheumatology*, **15**, 347–352.

Lentzsch, S., Gries, M., Janz, M., Bargou, R., Dörken, B. & Mapara, M.Y. (2003) Macrophage inflammatory protein 1-alpha (MIP-1 alpha) triggers migration and signaling cascades mediating survival and proliferation in multiple myeloma (MM) cells. *Blood*, **101**, 3568–3573.

Noll, J.E., Williams, S.A., Tong, C.M., Wang, H., Quach, J.M., Purton, L.E., Pilkington, K., To, L.B., Evdokiou, A., Gronthos, S. & Zannettino, A.C. (2014) Myeloma plasma cells alter the bone marrow microenvironment by stimulating the

© 2015 John Wiley & Sons Ltd

proliferation of mesenchymal stromal cells. *Haematologica*, **99**, 163–171.

Oyajobi, B.O., Franchin, G., Williams, P.J., Pulkrabek, D., Gupta, A., Munoz, S., Grubbs, B., Zhao, M., Chen, D., Sherry, B. & Mundy, G.R. (2003) Dual effects of macrophage inflammatory protein-1α on osteolysis and tumor burden in the murine 5TGM1 model of myeloma bone disease. *Blood*, **102**, 311–319.

Politou, M., Terpos, E., Anagnostopoulos, A., Szydlo, R., Laffan, M., Layton, M., Apperley, J.F., Dimopoulos, M.A. & Rahemtulla, A. (2004) Role of receptor activator of nuclear factor-kappa B ligand (RANKL), osteoprotegerin and macrophage protein 1-alpha (MIP-1a) in monoclonal gammopathy of undetermined significance (MGUS). *British Journal of Haematology*, **126**, 686–689.

Quinn, J., Glassford, J., Percy, L., Munson, P., Marafioti, T., Rodriguez-Justo, M. & Yong, K.L. (2011) APRIL promotes cell-cycle progression in primary multiple myeloma cells: influence of D-type cyclin group and translocation status. *Blood*, **117**, 890–901.

Rabin, N., Kyriakou, C., Coulton, L., Gallagher, O.M., Buckle, C., Benjamin, R., Singh, N., Glassford, J., Otsuki, T., Nathwani, A.C., Croucher, P.I. & Yong, K.L. (2007) A new xenograft model of myeloma bone disease demonstrating the efficacy of human mesenchymal stem cells expressing osteoprotegerin by lentiviral gene transfer. *Leukemia*, **21**, 2181–2191.

Rajkumar, S.V., Dimopoulos, M.A., Palumbo, A., Blade, J., Merlini, G., Mateos, M.-V., Kumar, S., Hillengass, J., Kastritis, E., Richardson, P., Landgren, O., Paiva, B., Dispenzieri, A., Weiss, B., LeLeu, X., Zweegman, S., Lonial, S., Rosinol, L., Zamagni, E., Jagannath, S., Sezer, O., Kristinsson, S.Y., Caers, J., Usmani, S.Z., Lahuerta, J.J., Johnsen, H.E., Beksac, M., Cavo, M., Goldschmidt, H., Terpos, E., Kyle, R.A., Anderson, K.C., Durie, B.G.M. & San Miguel, J.F. (2014) International Myeloma Working Group updated criteria for the diagnosis of multiple myeloma. *Lancet Oncology*, **15**, e538–e548.

Roodman, G.D. (2009) Pathogenesis of myeloma bone disease. *Leukemia*, **23**, 435–441.

Roodman, G.D. (2011) Osteoblast function in myeloma. *Bone*, **48**, 135–140.

Short, B.J., Brouard, N. & Simmons, P.J. (2009) Prospective isolation of mesenchymal stem cells from mouse compact bone. *Methods in Molecular Biology*, **482**, 259–268.

Sprynski, A.C., Hose, D., Caillot, L., Réme, T., Shaughnessy, Jr, J.D., Barlogie, B., Seckinger, A., Moreaux, J., Hundemer, M., Jourdan, M., Meissner, T., Jauch, A., Mahtouk, K., Kassambara, A., Bertsch, U., Rossi, J.F., Goldschmidt, H. & Klein, B. (2009) The role of IGF-1 as a major growth factor for myeloma cell lines and the prognostic relevance of the expression of its receptor. *Blood*, **113**, 4614–4626.

Taube, T., Beneton, M.N., McCloskey, E.V., Rogers, S., Greaves, M. & Kanis, J.A. (1992) Abnormal bone remodelling in patients with myelomatosis and normal biochemical indices of bone resorption. *European Journal of Haematology*, **49**, 192–198.

Terpos, E., Dimopoulos, M.A., Sezer, O., Roodman, D., Abildgaard, N., Vescio, R., Tosi, P., Garcia-Sanz, R., Davies, F., Chanan-Khan, A., Palumbo, A., Sonneveld, P., Drake, M.T., Harousseau, J.L., Anderson, K.C., Durie, B.G. & International Myeloma Working Group. (2010) The use of biochemical markers of bone remodeling in multiple myeloma: a report of the International Myeloma Working Group. *Leukemia*, **24**, 1700–1712.

Uneda, S., Hata, H., Matsuno, F., Harada, N., Mitsuya, Y., Kawano, F. & Mitsuya, H. (2003) Macrophage inflammatory protein-1 alpha is produced by human multiple myeloma (MM) cells and its expression correlates with bone lesions in patients with MM. *British Journal of Haematology*, **120**, 53–55.

Valentin-Opran, A., Charhon, S.A., Meunier, P.J., Edouard, C.M. & Arlot, M.E. (1982) Quantitative histology of myeloma-induced bone changes. *British Journal of Haematology*, **52**, 601–610.

Vallet, S., Pozzi, S., Patel, K., Vaghela, N., Fulciniti, M.T., Veiby, P., Hideshima, T., Santo, L., Cirstea, D., Scadden, D.T., Anderson, K.C. & Raje, N. (2011) A novel role for CCL3 (MIP-1α) in myeloma-induced bone disease via osteocalcin downregulation and inhibition of osteoblast function. *Leukemia*, **25**, 1174–1181.

Vejlgaard, T., Abildgaard, N., Jans, H., Nielsen, J.L. & Heickendorff, L. (1997) Abnormal bone turnover in monoclonal gammopathy of undetermined significance: analyses of type I collagen telopeptide, osteocalcin, bone-specific alkaline phosphatase and propeptides of type I and type III procollagens. *European Journal of Haematology*, **58**, 104–108.

Woitge, H.W., Horn, E., Keck, A.V., Auler, B., Seibel, M.J. & Pecherstorfer, M. (2001) Biochemical markers of bone formation in patients with plasma cell dyscrasias and benign osteoporosis. *Clinical Chemistry*, **47**, 686–693.

Yan, Y., Tang, D., Chen, M., Huang, J., Xie, R., Jonason, J.H., Tan, X., Hou, W., Reynolds, D., Hsu, W., Harris, S.E., Puzas, J.E., Awad, H., O'Keefe, R.J., Boyce, B.F. & Chen, D. (2009) Axin2 controls bone remodeling through the β-catenin–BMP signaling pathway in adult mice. *Journal of Cell Science*, **122**, 3566–3578.

© 2015 John Wiley & Sons Ltd